Separation Science and Technology
Publication details, including instructions for authors and subscription information:
http://www.informaworld.com/smpp/title~content=t713708471

High-Pressure Gas Chromatography and Chromatography with Supercritical Fluids. II. Permeability and Efficiency of Packed Columns with High-Pressure Gases as Mobile Fluids under Conditions of Incipient Turbulence

S. T. Sie[a]; G. W. A. Rijnders[a]
[a] KONINKLIJKE/SHELL-LABORATORIUM, AMSTERDAM, NETHERLANDS

To cite this Article Sie, S. T. and Rijnders, G. W. A.(1967) 'High-Pressure Gas Chromatography and Chromatography with Supercritical Fluids. II. Permeability and Efficiency of Packed Columns with High-Pressure Gases as Mobile Fluids under Conditions of Incipient Turbulence', Separation Science and Technology, 2: 6, 699 — 727
To link to this Article: DOI: 10.1080/01496396708049734
URL: http://dx.doi.org/10.1080/01496396708049734

SEPARATION SCIENCE, 2(6), pp. 699–727, Dec., 1967

High-Pressure Gas Chromatography and Chromatography with Supercritical Fluids. II. Permeability and Efficiency of Packed Columns with High-Pressure Gases as Mobile Fluids under Conditions of Incipient Turbulence

S. T. SIE and G. W. A. RIJNDERS

KONINKLIJKE/SHELL-LABORATORIUM, AMSTERDAM (SHELL RESEARCH N.V.)
NETHERLANDS

Summary

The behavior of packed gas-liquid chromatographic columns using carbon dioxide as a carrier gas has been studied at various pressures.

Measurements of pressure drop as a function of flow rate indicated that at velocities normally used in gas chromatography the flow through the column becomes progressively more turbulent with increasing pressures above a few atmospheres. At conditions near the critical pressure the Reynolds number may be about three orders higher than in normal gas chromatography with hydrogen or helium as a carrier gas.

Measurements of column efficiency at various gas pressures and velocities disclosed that the most important contributions to plate height (at pressures higher than usual in gas chromatography) are associated with large-scale unevenness of flow and intraparticle gaseous diffusion, respectively.

From a comparison of high-pressure gas chromatography with conventional gas chromatography and liquid chromatography, it appears that as regards potential speed and efficiency the two first-mentioned techniques are comparable and much better than the last one.

Our previous work (*1*) has shown that deviations from perfect gas behavior have an appreciable effect on partition coefficients in gas-liquid chromatography at higher pressures. For instance, with carbon dioxide as a carrier gas at 40°C and 80 atm, molecular interactions in the gas phase have been found to cause an apparent increase in volatility by a factor of 10 or more. Much larger effects

are to be expected at pressures well above the critical value (for CO_2: 73 atm), especially for heavy solutes. High-pressure gas chromatography has, therefore, the potential of extending the range of applicability of gas chromatography to heavier substances.

The separating ability of a chromatographic system for a pair of substances is directly related to the difference in partition coefficients and the number of theoretical plates of the column. The effect of gas pressure on the partition coefficient was dealt with in our previous paper (*1*). The present study is concerned with the column performance and more specifically with the effects of gas pressure, flow rate, and column parameters on plate height.

Besides plate-height studies we also carried out some measurements of the resistance to flow of the chromatographic column to gain some insight into flow conditions. Another incentive for such measurements is the consideration that pressure drop is an important factor in chromatography, because it may, under certain circumstances, set a limit to the speed of analysis as well as the separating efficiency attainable within a given practical time limit (*2,3*).

As packed columns represent the type most commonly used in both gas and liquid chromatography, we have restricted our study to this type of column.

EXPERIMENTAL

Measurements of Plate Height and Permeability of Columns

The apparatus used is suitable for experiments at working pressures up to 80 atm. It has been described in detail previously (*1*). Basically, it contains the same components as in normal GLC, viz., a gas feed system, an injection device, the column, a detector for detecting eluted components, and means for controlling and measuring pressures, flow rates, and temperature.

All measurements were carried out at 40°C. Carbon dioxide was the carrier gas in most of the experiments. A few measurements were performed with hydrogen.

We used conventional GLC columns (mostly 6 mm i.d., 1 m length) with a packing of Sil-O-Cel C22 firebrick (Johns-Manville Corporation), coated with squalane. Columns were filled and coiled in the usual way. Relevant properties of the columns investigated

TABLE 1

Some Properties of Columns Investigated[a]

	Column designation				
	A	B	C	D	E
Inner diameter, mm	6	6	6	6	3
Mesh size of support	50–70	50–70	80–100	100–120	120–200
Mean sieve diameter, mm	0.25	0.25	0.16	0.14	0.10
Filling density, g of dry support/ml of bed	0.394	0.390	0.423	0.429	0.451
Fractional volume of support skeleton, ml/ml of bed	0.183	0.181	0.197	0.199	0.210
Fractional volume of liquid, ml/ml of bed	0.145	0.143	0.158	0.161	0.169
Fractional gas volume, ml/ml of bed	0.672	0.676	0.645	0.640	0.621
Intergranular porosity[b]	0.375	0.381	0.327	0.319	0.285
Intragranular porosity[c]	0.297	0.295	0.318	0.321	0.336

[a] Common properties: column length, 100 cm; diameter of coil, 10 cm; support, Sil-O-Cel C22; stationary liquid, squalane; liquid/support weight ratio, 30/100.
[b] Volume of channels between granules per unit volume of bed.
[c] Volume of gas-filled pore space within granules per unit volume of bed.

are collected in Table 1. The manner in which they were determined is described in the next section.

Pressure drop across a column was measured by means of a differential manometer (range 0–500-cm water column), suitable for static pressures up to at least 100 kg/cm² (Barton Europa N.V.). This manometer was checked against a mercury U-tube manometer at 1 and 60 kg/cm² and found to be accurate within 0.005 kg/cm² at both pressure levels.

Fluid velocity was determined in two independent ways. One method consists in measuring the volumetric flow rate of gas after expansion to atmospheric pressure by means of a soap-film flowmeter or a wet-test meter. The atmospheric flow rate is converted to column temperature and average column pressure with the aid of compressibility data taken from the literature (*4,5*). In the permeability correlations, the arithmetic means of inlet and outlet pressure are adopted as the average column pressure, and the velocity is expressed as the average nominal velocity $\bar{u}$ calculated on the

empty tube. In the studies of solute retention and plate height, we used the average interstitial velocity $\bar{v}$, which is based on the average column pressure according to James and Martin* and the total cross-sectional area available to the gas.

The second, more direct way of measuring $\bar{v}$ consists in determining the mean holdup time of a nonpartitioning component. For this purpose methane is employed, a small correction being made for the finite solubility in the stationary liquid [see (*1*)]. In general, the results of the methods showed good agreement.

Plate-height measurements were conducted with methane, propane, and *n*-pentane as solutes. Care was taken to minimize dead volumes between sample inlet and column, and between the latter and the detector. The sample (about 15 μl of gas) was injected with a pneumatically operated injection device. The detection principle used was flame ionization.

The exact moment of injection was marked on the recorder chart by means of a microswitch arrangement. We used chart speeds up to 480 in./hr to allow accurate measurements of peak distances and widths. The contribution of the amplifier and recorder response times to recorded peak width can be considered to be negligible, except for the narrowest methane peaks approaching a width of 1 sec.

Series of plate-height and permeability measurements were repeated on several occasions in a more or less random way to see if geometrical changes had occurred in the columns. This proved not to be the case.

Determination of Inter- and Intragranular Porosities of Column Packing

The apparent density of Sil-O-Cel C22 firebrick was determined by measuring the size of whole bricks, which were then dried and weighed. Making a slight correction for cracks and voids, we found an apparent density of 0.63 g/cm^3.

The true specific gravity (density of the silica skeleton) is given by the manufacturers (*6*) as 2.15 g/cm^3. Hence, per cubic centimeter

* $\bar{P} = \frac{2}{3}\{[P_i/P_o)^3 - 1]/[(P_i/P_o)^2 - 1]\}\ P_o$, where P_i is the inlet and P_o the outlet pressure. The distinction between the average pressure thus defined and the arithmetic mean pressure is only of importance in the experiments at atmospheric outlet pressure. Even here the differences are small; for instance, at a P_i/P_o ratio of 1.5 it amounts to less than 2%.

of particle the skeleton occupies a volume of 0.293 cm^3, while the pores account for the remaining 0.707 cm^3. The specific pore volume is thus found to be 1.12 cm^3/g. These values agree well with the ones reported by Baker et al. (7) for Chromosorb R, which is essentially the same material. The specific pore volume found by these authors is 1.1 cm^3/g, while the skeleton density is reported as 2.26 g/cm^3.

The liquid-to-support weight ratio was determined by weighing. From the weight of the column packing (obtained by weighing the empty and filled columns) and the inner volume of the empty column, the weights of dry Sil-O-Cel and liquid phase per unit volume of bed were derived. From the apparent particle density (0.63 g/cm^3), the skeleton density (2.15 g/cm^3) and the liquid density (0.801 g/cm^3 at 40°C), we calculated the particle volume, the volume occupied by the silica skeleton, and the liquid volume (all per unit volume of bed). Subtraction of the fractional particle volume from unity gave the intergranular porosity (volume of channels per unit volume of bed). Subtraction of the fractional volumes of skeleton and liquid from the fractional particle volume gave the intraparticle porosity of the packing (volume of intraparticle pores per unit volume of bed).

TABLE 2

Coefficients of Diffusion (calculated values)

Substance	Medium	State	Temperature, °C	Pressure, kg/cm^2	Diffusivity, cm^2/sec
Methane	CO_2	Gas	40	1	0.157[a]
Propane	CO_2	Gas	40	1	0.091
n-Pentane	CO_2	Gas	40	1	0.077
n-Pentane	H_2	Gas	40	1	0.27
Methane	CO_2	Gas	40	57	1.9×10^{-3}
Propane	CO_2	Gas	40	57	1.0×10^{-3}
n-Pentane	CO_2	Gas	40	57	8.4×10^{-4}
Methane	Squalane	Liquid	40	—	4.1×10^{-6}
Propane	Squalane	Liquid	40	—	2.2×10^{-6}
n-Pentane	Squalane	Liquid	40	—	1.6×10^{-6}

[a] This value compares reasonably well with an experimental value of 0.154 cm^2/sec for the diffusivity of methane in CO_2 at atmospheric pressure and 0°C (*11*).

Diffusivities and Other Data

Diffusivities in gases at atmospheric pressure were estimated with the aid of the correlation formula of Gilliland (*8*). Diffusivities in gases at higher pressures, where deviations from perfect gas behavior become apparent, were calculated on the basis of Enskog's theory of dense gases (*9*). Liquid diffusivities were estimated by means of the correlation formula of Arnold (*10*). The values used in subsequent calculations are collected in Table 2.

Partition coefficients were determined in the way described earlier (*1*). Figures for the viscosity and density of carbon dioxide at various pressures and temperatures as well as other data were taken from the literature (*4,5,11*).

RESULTS AND DISCUSSION

Column Permeability

Development of Turbulence at Higher Pressures. In laminar flow the relation between the pressure gradient and the local velocity in a packed tube is a linear one (*12,13*), viz.,

$$u_x = -K\left(\frac{dP}{dx}\right)_x \tag{1}$$

where K is a constant (permeability) and x is the coordinate along the tube axis. If the permeability does not vary along the column length and if the fluid behaves as an ideal gas,* Eq. (1) can be written as

$$u_o \frac{P_o}{P_x} = -K\left(\frac{dP}{dx}\right)_x$$

where the index o denotes the column outlet. Integrating the above equation along the column length, we obtain

$$u_o P_o L = \tfrac{1}{2}K(P_i^2 - P_o^2) = \tfrac{1}{2}K(P_i - P_o)(P_i + P_o)$$

in which the index i denotes the column inlet and L is the column length. Since $u_o P_o / \tfrac{1}{2}(P_i + P_o)$ is the average nominal velocity $\bar{u}$ (see

* This is, of course, no longer true at high pressures. At such pressures, however, the small pressure drop (<0.5 kg/cm²) hardly causes any expansion and the fluid velocity hardly varies along the column length. In this case, Eq. (1a) is obtained directly by integrating Eq. (1).

experimental section), the relation between the overall pressure drop ΔP and $\bar{u}$ becomes

$$\bar{u} = K\frac{\Delta P}{L} \tag{1a}$$

The validity of this relation was examined for a column packed with 50/70 mesh Sil-O-Cel (column A, see Table 1) at varying outlet pressures. As will be seen from Fig. 1, the expected linear relationship for laminar flow proved to hold only for the series of measurements at an outlet pressure of 1 kg/cm², and even here this seems to be restricted to velocities below 10 cm/sec. At higher flow rates and especially at higher pressures, the curves assume a parabolic shape (concave toward the ΔP axis).

The above observations can be understood by considering the Reynolds numbers involved ($d_p\bar{v}\rho/\eta$, where d_p is the mean par-

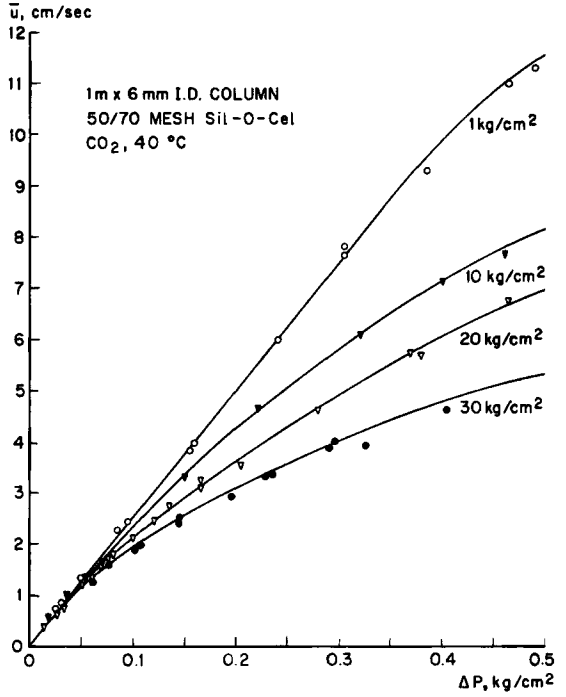

FIG. 1. Relation between average nominal velocity and pressure drop at various outlet pressures.

ticle diameter, ρ the fluid density, and η the dynamic viscosity). For the present column a carbon dioxide velocity of 10 cm/sec at atmospheric pressure corresponds to a Reynolds number of 3.

As the transition from laminar flow to turbulence is known to occur at a Reynolds number of the order of 1 in packed beds, it is conceivable that turbulence develops at higher velocities.

From the kinetic theory of gases it follows that at constant temperature viscosity is independent of pressure, while density is proportional to it; hence, ρ/η increases with pressure. This explains why at the velocities considered flow becomes increasingly nonlaminar at higher pressures.

For CO_2 near the critical pressure ρ/η attains values of more than 1000 sec/cm^2, i.e., three orders higher than for carrier gases mostly used in GLC (viz., about 1 sec/cm^2 for H_2 and He at 1 atm). It is of interest to note that the value of ρ/η is also considerably higher for supercritical CO_2 than for liquids commonly employed in liquid chromatography, e.g., 99 for water, 101 for pyridine, 167 for *n*-heptane, 135 for benzene, and 66 for methanol (all values in seconds per square centimeter at room temperature). This is probably true for supercritical fluids in general.*

We may conclude, therefore, that turbulent flow conditions are obtained far more easily with high-pressure gases or supercritical fluids than with the conventional mobile fluids, i.e., low-pressure gases and liquids.

Permeability in the Laminar Region. From the slope of the linear portion of the ΔP-$\bar{u}$ curves in Fig. 1, the specific surface contributing to frictional resistance for laminar flow may be calculated by means of the Kozeny-Carman equation (*12*):

$$\bar{u} = \frac{\epsilon^3}{5\eta S_v^2(1-\epsilon)^2}\frac{\Delta P}{L} \qquad (1b)$$

where ϵ is the interparticle porosity, L the column length, and S_v the specific surface per unit volume of particle.

Thus substituting $\Delta P/\bar{u} = 3.9 \times 10^4$ dyne-sec/cm^3, $L = 100$ cm, $\epsilon = 0.375$ (intergranular porosity), and $\eta = 1.57 \times 10^{-4}$ dyne-sec/cm^2, we obtain for S_v a value of 260 cm^{-1}.

* If a supercritical fluid is regarded as a liquid heated under pressure above its critical temperature, it is plausible that ρ/η should be higher at supercritical conditions, since viscosity drops more rapidly than density with increasing temperature.

Since for a sphere $S_v = 6/d$ (d = sphere diameter), the equivalent sphere diameter d_s is

$$d_s = \frac{6}{260} = 2.3 \times 10^{-2} \text{ cm}$$

This is only slightly lower than the actual mean particle diameter (as follows from sieve analysis), viz., $d_p = 2.5 \times 10^{-2}$ cm.

Although no great weight attaches to the difference between d_s and d_p, it may mean that the porous Sil-O-Cel packing examined offers a slightly higher resistance to flow than an equally close-packed bed of solid spheres of the same average diameter. This result is in good agreement with those obtained by Dal Nogare and Jen Chiu (*14*), who found about 20% more resistance to flow (as compared with spheres) for silanized Chromosorb R.

Permeability in the Nonlaminar Region. The resistance coefficient ψ from the correlation formula of Rose and Rizk (*15,16*), defined by

$$\left(\frac{\Delta P}{\rho g d_s}\right) = \psi \left(\frac{\bar{u}^2}{d_s g}\right)\left(\frac{L}{d_s}\right) \varphi_1(\epsilon)\varphi_2\left(\frac{D}{d_s}\right) \qquad (2)$$

has been calculated from experimental ΔP and $\bar{u}$ values, taking

$$d_s = d_p = 250\ \mu$$

$$\varphi_1(\epsilon) = 1.20$$

$$\varphi_2\left(\frac{D}{d_s}\right) = 1.05$$

In the above equations g is the gravity constant, D the tube diameter, and φ denotes "function of."

The values of φ_1 (porosity function) and φ_2 (wall effect), as given above, were determined from the graphical correlations of Rose and Rizk (*16*). In taking $d_s = d_p$, we have assumed the particles to be solid spheres.

In Fig. 2 log ψ has been plotted against the logarithm of the Reynolds number for the experimental results of Fig. 1 as well as some additional results at higher pressures. From this figure it can be concluded that the hydrodynamic behavior of the Sil-O-Cel packing is also comparable to that of a bed of solid particles in the nonlaminar region.

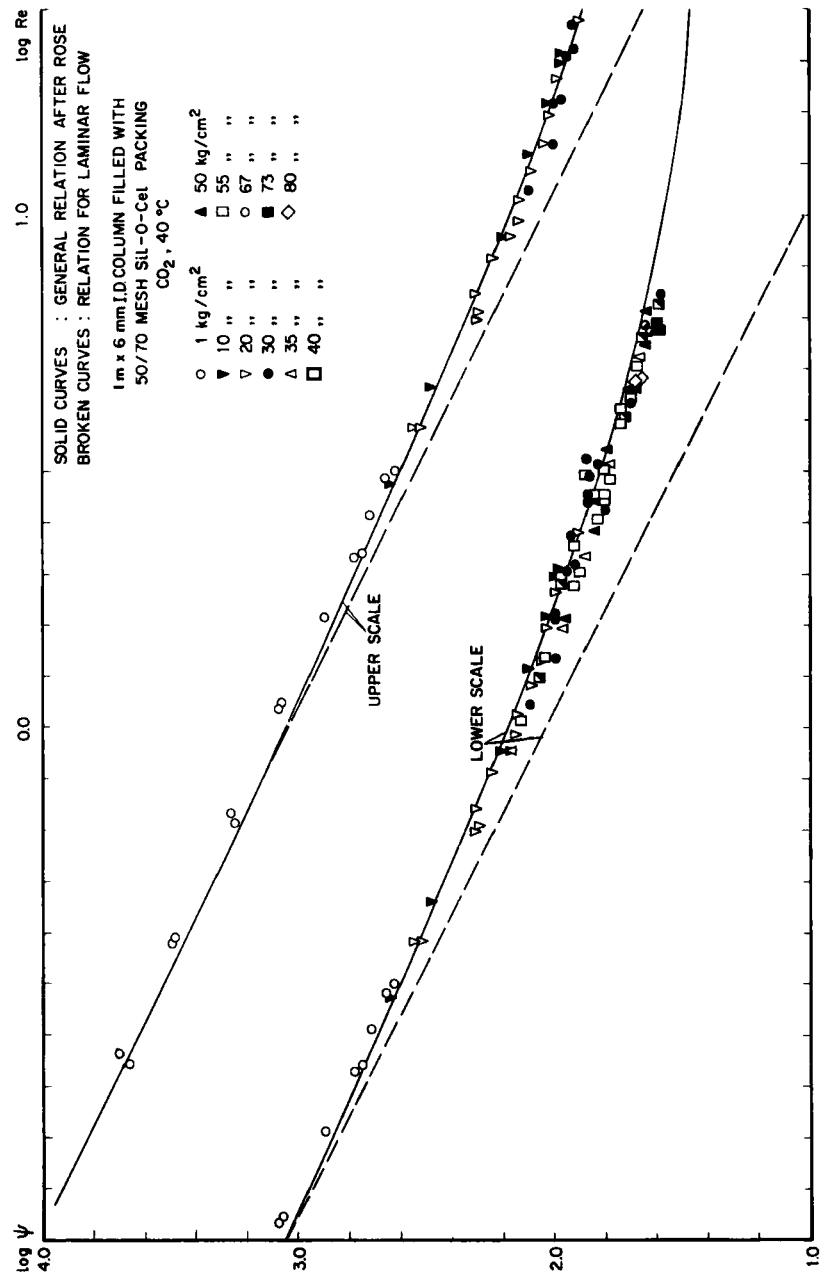

FIG. 2. Relation between resistance coefficient and Reynolds number showing transition from laminar to turbulent flow.

Column Efficiency in GLC at Various Pressures

Plate-Height Curves at Atmospheric Outlet Pressures. Figures 3 and 4 present some results of plate-height measurements under normal GLC conditions. It will be seen that in all cases examined, the experimental points closely fit an equation of the van Deemter type:

$$H = A + B/\bar{v} + C\bar{v} \tag{3}$$

where H is the plate height and A, B, and C are constants.

Two points are of interest here: (1) at these low pressures the "eddy-diffusion" term A is zero within experimental error, and (2) the coefficient of the "nonequilibrium" term C for *n*-pentane is of the same order of magnitude for all curves. Evidently, the term C does not depend very much on the size of the packing or on the nature of the carrier gas. We shall revert to these points later.

Effect of Pressure on the Constants of the van Deemter Equation. Figures 5 and 6 present the results of measdrements carried out at different pressures up to 50 kg/cm²* with carbon dioxide as the carrier gas and propane and *n*-pentane as solutes. The effect of pressure on

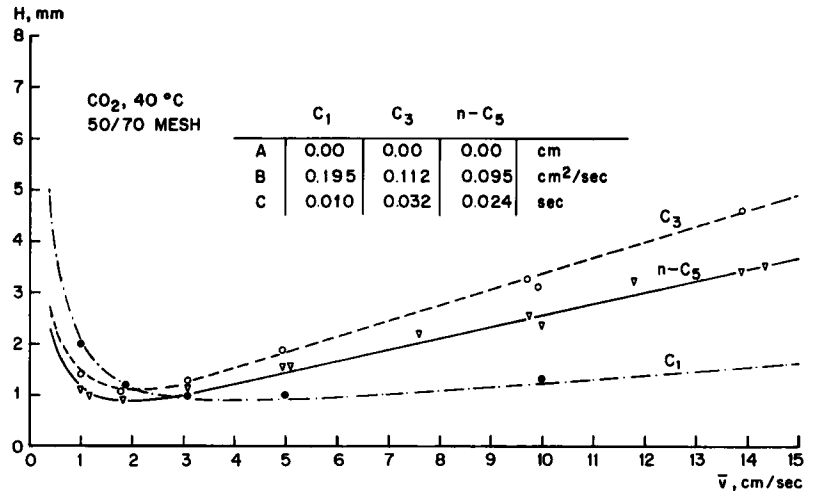

FIG. 3. Plate-height curves at atmospheric outlet pressure for column A. Curves represent the relation $H = A + B/\bar{v} + C\bar{v}$.

* At the higher pressure levels the pressure drop across the column can be neglected, so that it is not necessary to distinguish between inlet, outlet, and mean column pressure.

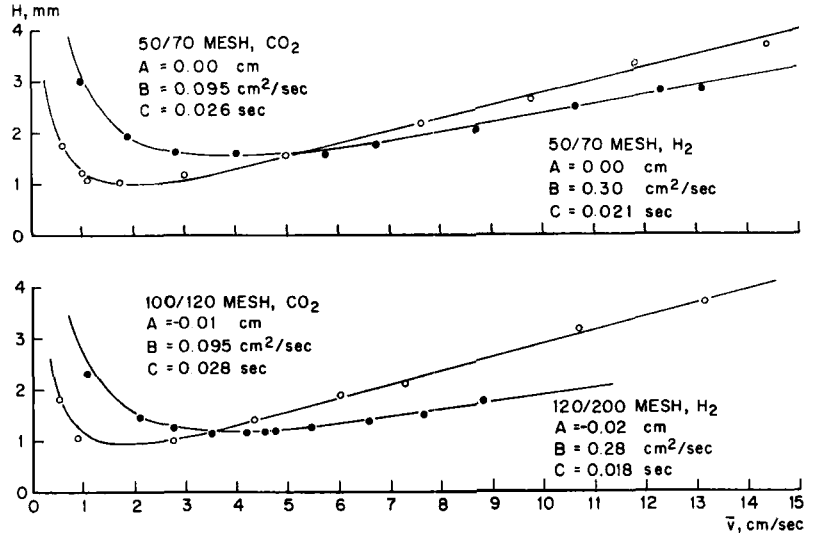

FIG. 4. Plate-height curves at atmospheric outlet pressure for columns B, D, and E. Solute, *n*-pentane; *T*, 40°C. Curves represent the relation $H = A + B/\bar{v} + C\bar{v}$.

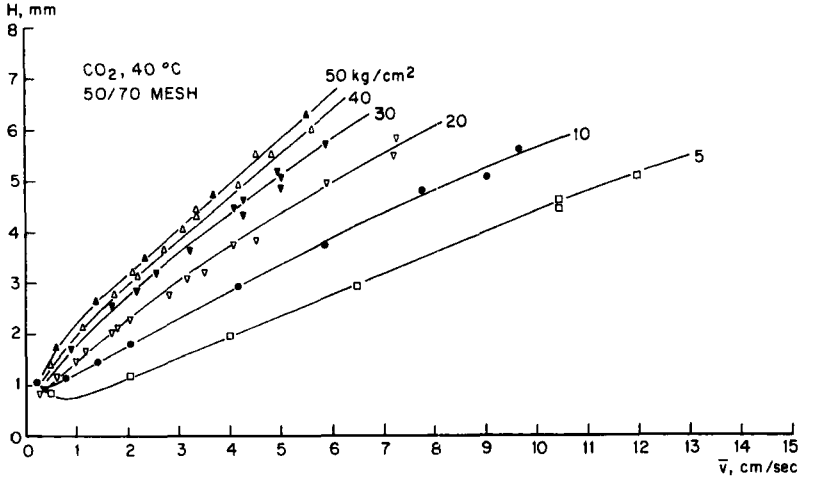

FIG. 5. Effect of carrier gas pressure on the plate-height curve. Propane as a solute on column A.

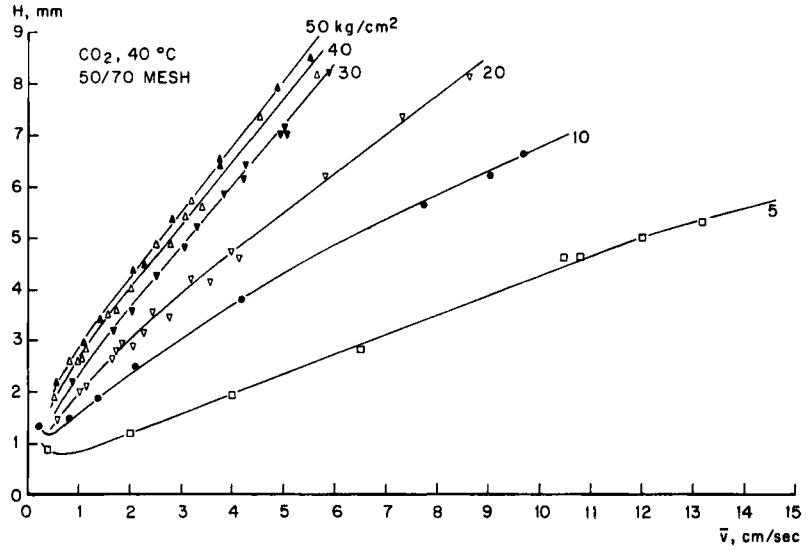

FIG. 6. Effect of carrier gas pressure on the plate-height curve. *n*-Pentane as a solute on column A.

the partition coefficients of these solutes is shown in Fig. 7. Before trying to explain the shape of the plate-height curves at higher pressures (which we shall do in a later section), we shall for the moment discuss these curves phenomenologically. In particular, we shall examine what is the fate of the *A*, *B*, and *C* terms if the pressure is increased.

a. Eddy-Diffusion Contribution (A Term). As stated before, *A* is zero within experimental error under normal GLC conditions. If the eddy-diffusion contribution is obtained as the intercept of the "straight" part of the plate-height curve on the *H* axis (as is commonly done), it is evident that *A* is no longer zero at higher pressures, e.g., at 50 kg/cm² (see Figs. 5 and 6). This also follows from Figs. 9 and 10 (pertaining to experiments to be discussed later). These curves are to be compared with those in Fig. 4 for the same columns.

The above observation is at variance with the classical idea that eddy diffusivity (spreading due to statistical variations of velocity within the packed bed) contributes as an additive constant which only depends on packing geometry and particle dimensions.

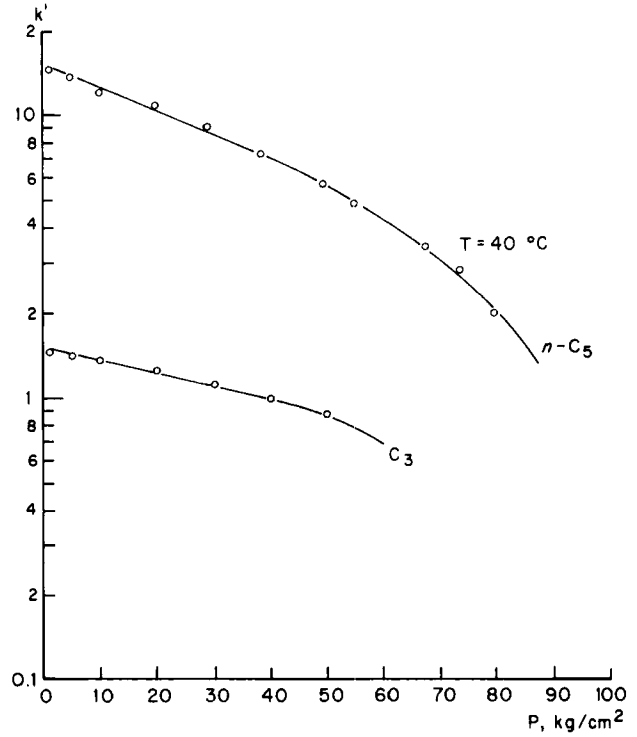

FIG. 7. Effect of carbon dioxide pressure on partition coefficients of propane and *n*-pentane (Column A).

b. Longitudinal Molecular Diffusion (B Term). In the van Deemter equation B is equal to $2\gamma D_g$, where γ is a tortuosity factor and D_g the molecular diffusivity in the gas phase. Since the latter diminishes with pressure, the B term must become smaller at higher pressures. As can be seen from Figs. 3, 5, and 6, this proves to be true, the minimum plate height apparently shifting to lower velocities, as the pressure is higher.

Above 10 kg/cm² the ascending branch at lower velocities is no longer discernible in the velocity range considered. At such pressures and at the velocities with which we are mostly concerned (i.e., $\bar{v} > 2$ cm/sec), the contribution of longitudinal molecular diffusion is relatively unimportant and can, for all practical purposes, be neglected.

c. Nonequilibrium Contribution (C Term). As reflected in the slope of the curves in Figs. 5 and 6, the nonequilibrium contribution increases with increasing pressures and becomes by far the

most important factor in determining column efficiency at high pressures and velocities. It is noteworthy that the deterioration of column efficiency with increasing pressure is very rapid in the beginning, but slackens off at higher pressures. Also, the curves for pressures above 5 kg/cm² appear to be concave with respect to the $\bar{v}$ axis, although it is difficult to determine their exact shape unambiguously.

Relative Magnitude of the Gas- and Liquid-Phase Contributions to the Nonequilibrium Term Under Normal GLC Conditions. For a better understanding of the effect of pressure, it is of interest to examine in more detail the nature of the nonequilibrium term under normal GLC conditions. Variation of D_g—either by changing average column pressure or the nature of the carrier gas—allows C to be split up into the respective contributions of the two phases (C_l and C_g), which are assumed to be additive. In the low-pressure region, D_g can be taken to be inversely proportional to pressure, while changes in partition coefficients, liquid volume, and liquid diffusivity (caused by dissolved carrier gas) are still negligible.

Thus, from results obtained on column A at 1 and 5 kg/cm² outlet pressures (Figs. 3, 5, and 6), the following figures are obtained:

For propane as a solute: $C_l = 0.029$ sec
$C_g = 0.003$ sec (CO_2, 1 kg/cm²)
For *n*-pentane as a solute: $C_l = 0.019$ sec
$C_g = 0.005$ sec (CO_2, 1 kg/cm²)

The results for *n*-pentane are in good agreement with the figures calculated for the duplicate column (B) from the experiments with hydrogen and carbon dioxide as carrier gases at atmospheric outlet pressure (Fig. 4):

$C_l = 0.019$ sec
$C_g = 0.007$ sec (CO_2, 1 kg/cm²)

It follows that for the columns considered the liquid contribution is the more important one at atmospheric pressure. However, the gas-phase contribution cannot be ignored completely. It rapidly gains importance with increasing pressure and becomes the major contributor at pressures of 10 kg/cm² and above.

Liquid Contribution. The dominating role of the liquid contribution at low pressures is also reflected in the slopes of the high-velocity part of the curves in Fig. 3, which is lowest for methane

and highest for propane. From the well-known expression for C_l, viz.,

$$C_l = \frac{2}{3} \frac{k'}{(1+k')^2} \frac{d_l^2}{D_l} \tag{4}$$

where k' is the capacity ratio (partition coefficient multiplied by phase ratio), D_l the liquid diffusivity, and d_l the "effective liquid film thickness," it follows that C_l should be a maximum for $k' = 1$ and zero for $k' = 0$. These conditions approximately apply to propane and methane, respectively (k' for methane, propane, and *n*-pentane: 0.1, 1.6, and 15, respectively).

Using estimated diffusivities as given in Table 2, we calculate the effective liquid film thickness from the above expression to be 8.8 μ (from *n*-pentane data) and 6.4 μ (from propane data), which values do not appear to be very unrealistic for the relatively highly loaded columns. For a column packed with 10 wt. % dinonyl phthalate on Chromosorb P, Saha and Giddings (*17*) found the effective liquid thickness to be 2.5 μ.

If size reduction of the support does not substantially affect the pore-size distribution, it is plausible that Sil-O-Cel particles of different size have a similar inner structure and will have the liquid distributed in about the same way, if loaded to the same extent with stationary phase. Hence, we may expect that in the range considered, d_l, and therefore also C_l, will not vary much with particle size for a given liquid-to-support ratio.* This reasoning, combined with the preponderance of the liquid contribution at low pressures, lends support to our earlier observation about C being nearly independent of particle size and carrier gas under normal GLC conditions. For the experiment with *n*-pentane on column E (Fig. 4), where a fine packing is used in conjunction with a narrow column and hydrogen as the carrier gas, C_g should be very small, in fact much smaller than 0.005 sec (value found for column A with CO_2

* Saha and Giddings (*18*) found a significant effect of particle size on C_l with low-loaded Chromosorb G. They also showed that Chromosorb W of different size may have a somewhat different pore-size distribution which could lead to a similar dependence of C_l on particle size (*17*). However, these materials differ from Sil-O-Cel in the use of flux in their preparation, which could more easily cause the existence of parts of different porosity and friability. Whereas Sil-O-Cel or Chromosorb P consists of a more or less uniform dense mass of sintered diatomite particles, Chromosorb W is known to consist of diatomite fragments held together by a glassy phase (*19*).

carrier). The value found for C, viz., 0.018 sec, should be practically equal to C_l in this case. It actually agrees well with C_l found on columns A and B (0.019 sec).

Nature of the Gas-Phase Contribution to the Nonequilibrium Term at Low Pressures. *a. Interparticle Diffusion.* The contribution of the resistance against mass transfer originating from slowness of diffusion within the gas-filled channels of the packed bed (which may be called the interparticle gas-phase contribution) has been expressed by van Deemter (*20*) as

$$(C_g)_{\text{interparticle}} \simeq 0.01 \frac{(k')^2}{(1+k')^2} \frac{dp^2}{D_g} \tag{5}$$

For *n*-pentane as a solute on column A or B operated with CO_2 carrier at atmospheric outlet pressure, it follows from the above expression that $(C_g)_{\text{interparticle}}$ is about 7×10^{-5} sec. This value is smaller by about two orders of magnitude than the experimental values found for C_g, viz., 0.005 sec (column A) and 0.007 sec (column B). Although the numerical constant in the above expression is only approximate [its magnitude has been assessed from experimental mass-transfer data correlated by Ergun (*21*)], the expression should give at least the right order of magnitude for the interparticle gas-phase contribution.* Therefore, the discrepancy noted above must be considered significant and leads to the conclusion that the major part of C_g cannot originate from the limited rate of mass transport within the channels.

The above conclusion can also be drawn from results of other workers who have determined C_g values for packed columns, e.g., from the work of Kieselbach (*23*), Bohemen and Purnell (*24*), Deford et al. (*25*), Giddings and Schettler (*26*), and Perrett and Purnell (*27*).

b. Intraparticle Gaseous Diffusion. As a second contributor to C_g we may examine the effect of the finite rate of diffusion within the gas-filled pores inside the particles (intraparticle gas-phase contribution), which may be calculated from the equation:

$$(C_g)_{\text{intraparticle}} \simeq \frac{1}{30} \frac{(1+k'-\phi)^2}{(1+k')^2(1-\phi)} \frac{q}{\epsilon_p} \frac{d_p^2}{D_g} \tag{6}$$

* The contribution of interparticle gas-phase diffusion can also be estimated by a comparison of the packed bed with a capillary of the same hydraulic radius, using the formula of Golay (*22*). Such an estimation leads to an interparticle gas-phase contribution of the same magnitude as obtained from Eq. (5) [cf. Perrett and Purnell (*27*)].

In this formula [which is a slightly modified version of the one derived by Giddings (*28*)] ϕ is the fraction of gas occupying interparticle space, ϵ_p the porosity of the particle (i.e., volume of intraparticle gas space per unit volume of particle), and q a "tortuosity" factor.*

Substituting $\phi = 0.56$, $\epsilon_p = 0.48$, $d_p = 0.025$ cm (see data for columns A and B in Table 1) and taking $q = 1.3$,† we obtain for *n*-pentane as a solute, with CO_2 of atmospheric pressure as a carrier gas ($k' = 15$, $D_g = 0.077$ cm²/sec):

$$(C_g)_{\text{intraparticle}} = 1.7 \times 10^{-3} \text{ sec}$$

This contribution, although substantially higher than the interparticle one, is still considerably lower than the value found for C_g (by a factor of 3 to 4). It can, therefore, only account for a relatively small part of the gas-phase nonequilibrium term.

c. Contribution of Nonuniformity of Flow. As we showed elsewhere (*30*), appreciable velocity differences usually occur in different parts of any column cross-sectional area, giving rise to a very important contribution to plate height. Such velocity differences, caused by differences in column permeability (e.g., between wall and inner sections), are of a more or less systematic nature (macroscopic flow profiles). These flow profiles cause a spread in residence time of fluid elements, which is, however, lessened by exchange of material in a lateral direction. This exchange can occur by molecular diffusion in the mobile phase as well as by a "convective diffusion," the latter resulting from the repeated division and mixing of fluid streams in the three-dimensional network formed by the interstitial channels.

As demonstrated in another paper (*30*), the contribution of a flow profile to plate height (h) in laminar flow can be adequately described by

* The molecular diffusivity in the free space is multiplied by a factor ϵ_p/q to account for the fact that the pores are tortuous and occupy only part of the particle volume [see, e.g., (*29*)]. It is probable that in the present case the effective diffusivity in the particle can thus be compared with the normal molecular diffusivity (rather than be described as a Knudsen diffusion) since the pore diameters in Sil-O-Cel are larger than the molecular mean free path [average pore diameter about 1 μ (*7*); mean free path in CO_2 of 1 atm at 40°C about 6×10^{-6} cm]. This applies *a fortiori* to the experiments at high pressures.

† This value is of the same order of magnitude as the usual tortuosity correction factors for diffusion in packed beds. It corresponds with a γ value (B term in the van Deemter equation) of 0.77.

$$h = \frac{2\kappa R^2}{\lambda_R d_p \bar{v} + \gamma_R D_g} \bar{v} \tag{7}$$

where κ is a dimensionless parameter pertaining to the profile, R the tube radius, and λ_R and γ_R dimensionless constants depending upon packing geometry. In isotropic beds, γ_R is the same as the tortuosity factor in the B term of the van Deemter equation. The expression below the bar represents the lateral diffusivity, which is composed of a convective and a molecular part.

On the basis of various models of a randomly packed bed and experimental data, we have assessed a value of about $\frac{1}{30}$ for λ_R (*30*). With this value, the convective diffusivity ($\lambda_R d_p \bar{v}$) in column A or B ($d_p = 0.025$ cm) is calculated to be 0.004 cm²/sec at a velocity of 5 cm/sec. This is considerably smaller than the molecular diffusivity in CO_2 at atmospheric pressure ($\gamma_R D_g = 0.048$ cm²/sec for *n*-pentane, as follows from the B term of the curves in Figs. 3 and 4). If, therefore, we neglect the share of the convective mechanism in the lateral transport, the profile term reduces to

$$h = \frac{2\kappa R^2}{\gamma_R D_g} \bar{v}$$

or

$$(C_g)_{\text{profile}} = \frac{2\kappa R^2}{\gamma_R D_g} \tag{8}$$

Hence, at low pressures the packing irregularity does not contribute to plate height as a velocity-independent A term, but takes a share in the nonequilibrium term.

The magnitude of κ depends on the technique of packing, among other things. As shown elsewhere (*30*), columns packed by techniques common in GLC and of the size here considered mostly have κ values of about 10^{-3}.* For column A or B ($R = 0.3$ cm) this gives

$$(C_g)_{\text{profile}} = 3.8 \times 10^{-3} \text{ sec}$$

if *n*-pentane is used as a solute, with CO_2 as a carrier gas at atmospheric pressure ($\gamma_R D_g = 0.048$ cm²/sec).

* This roughly corresponds with velocity differences of the order of 10 or 20%, as have been shown to exist in preparative-size columns (*31*). Such differences can result from small variations in packing density or mean particle size (caused by segregation) in different parts of the column. For instance, from the Kozeny-Carman equation it follows that variations of 0.01 in ϵ (at a level of 0.4) or 0.002 cm in d_p (at a level of 0.025 cm) suffice to produce such velocity differences in laminar flow.

It will be clear that the profile contribution is larger than the previously calculated intraparticle one (1.7×10^{-3} sec). If we add them together, the predicted value for C_g becomes 5.5×10^{-3} sec, which compares very well with the values actually found (5×10^{-3} and 7×10^{-3} sec).

Although the excellent agreement may be partly fortuitous, it is nevertheless clear that the flow profile contribution can fill the previously existing gap between theory and experiment. It also appears to be the major contributor to C_g. The latter conclusion is not necessarily restricted to the present case, but may apply to conventional packed-column GLC in general, in agreement with a postulate by Littlewood (32).

Effect of Pressure on the Flow-Profile Contribution. As pointed out before, the nonequilibrium term increases with pressure, rapidly at first but more slowly at higher pressures (Figs. 5 and 6). This behavior cannot be understood if inter- and intraparticle diffusion were the sole contributors to C_g, in which case C_g should increase in inverse ratio to the diffusivity.* The reciprocal diffusivity increases in direct proportion to pressure at low pressures, but more sharply in the high-pressure nonideal regions (see Table 3), so that the expected course of C_g at high pressures is opposite to that actually observed.

The fact that C_g is mainly built up from the profile contribution does, however, provide a logical explanation for the experimental facts. At higher pressure the convective lateral diffusion ($\lambda_R d_p \bar{v}$) gains importance as the molecular diffusivity diminishes. When the former mechanism of lateral exchange dominates completely, Eq. (7) reduces to

$$h = \frac{2\kappa R^2}{\lambda_R d_p} \tag{9}$$

* The fact that turbulence develops at higher pressure does not invalidate this conclusion since the intraparticle contribution is much larger than the interparticle one. The former contribution is probably not affected much by turbulence. Moreover, although the interparticle term is expected to become smaller with turbulent flow (owing to promoted mass transfer), the reduction is not likely to be very dramatic. In a packed bed the transition from laminar to turbulent flow is gradual; the mass-transfer coefficient approximately following the same course as the resistance coefficient with increasing Reynolds number [see, e.g., (*21*)]. In the experiment with column A at 50 kg/cm² (Reynolds numbers ranging from about 7 to 70), the reduction of the interparticle contribution by turbulence may amount to, e.g., a factor of 1.1 to 1.5. Its effect on the overall C_g cannot, therefore, explain the fact that at 50 kg/cm² C_g is lower by a factor of at least 3 (as compared with a value obtained by extrapolating the low-pressure data).

TABLE 3

Velocities at which Lateral Convective Diffusivity Equals Molecular Diffusivity, as a Function of Pressure[a]

P, kg/cm²	D_g, cm²/sec	$\bar{v}$, cm/sec
1	7.7×10^{-2}	57
5	1.6×10^{-2}	12
10	7.6×10^{-3}	5.5
20	3.8×10^{-3}	2.8
30	2.3×10^{-3}	1.7
40	1.5×10^{-3}	1.1
50	1.1×10^{-3}	0.8
57	8.4×10^{-4}	0.6

[a] Carrier gas, CO_2; temperature, 40°C; solute, *n*-pentane; mean particle diameter, 0.025 cm (50/70 mesh); $\lambda_R = \frac{1}{30}$; $\gamma_R = 0.62$. The γ_R value follows from the B term of the respective plate-height relations in Figs. 3 and 4.

Hence, the contribution of a flow profile to plate height tends to become independent of velocity with increasing pressure and/or velocity. This explains the reduced rate of increase of C_g at higher pressures, as well as the fact that the plate-height curves of Figs. 5 and 6 are somewhat concave with respect to the $\bar{v}$ axis. The region of maximum curvature (where $\lambda_R d_p \bar{v}$ and $\gamma_R D_g$ are of the same order of magnitude) should shift to lower velocities accordingly as the pressure is higher (cf. Table 3), which is actually borne out by the curves in Figs. 5 and 6.

An explanation may now be offered, too, for the paradoxical fact that the A term is insignificant at low pressures, but considerable at high ones (see p. 711). Table 3 shows that at a pressure of 50 kg/cm² or higher and at velocities above, e.g., 3 cm/sec, the effect of packing inhomogeneity is no longer to be found in the C term (as in the experiments at atmospheric pressure) but rather in an A term.* With a value of 10^{-3} for κ and $\frac{1}{30}$ for λ_R (see preceding section), it follows from Eq. (9) that this A term should be about 2 mm for columns A and B. This compares well with values of 1.8 and 2.2 mm, as obtained by taking the intercept on the H axis of the

* This is, in essence, what the coupling theory of eddy diffusion of Giddings (33) predicts. Recently, Horne et al. (34), in studies on the axial dispersion of solute bands in unsorbing glass-bead columns, also showed that this dispersion becomes independent of velocity at Reynolds numbers in excess of about 10. They also concluded that the major factor producing such dispersion is the slowness of trans-column equilibration.

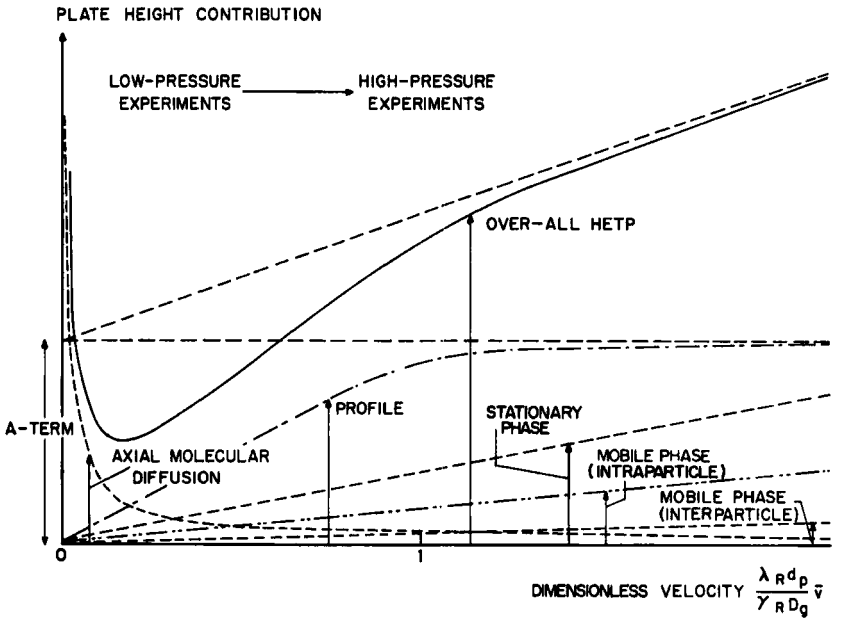

FIG. 8. Schematic representation of various plate-height contributions as a function of mobile fluid velocity (laminar flow).

"straight" parts of the high-pressure curves for *n*-pentane in Figs. 6 and 9.

The gradual shift in the working region caused by the increase in pressure is illustrated by Fig. 8, which is a schematic representation of the course of various plate-height contributions with increasing dimensionless velocity for laminar flow.

It will be clear that with the effect of pressure on the flow-profile contribution, as discussed above, it is possible to explain the most salient points about the shape of the plate-height curves at different pressures (Figs. 5 and 6) in a semiquantitative way at least. Although for a more rigorous test of the theory it would be desirable to examine how well our experimental data fit theoretically determined curves, such a test is rendered very difficult by the complications arising from turbulence and the solution of carrier gas in the stationary liquid.

Turbulence may affect the flow profile (velocity distribution) and the convective lateral diffusion as well. The solution of carrier gas in the stationary liquid [which has been shown to be appreci-

able for the present system; see (*1*)] may change the liquid volume as well as the liquid diffusivity.

Effect of Particle Size on Plate-Height at High Pressures and Velocities. As discussed above, flow profiles no longer contribute significantly to C_g at high pressures and velocities ($P > 50$ kg/cm², $\bar{v} > 3$ cm/sec). Since the contribution of interparticle diffusion has been shown to be small vis-à-vis that of intraparticle diffusion (which must be even more so for turbulent flow), it follows that only the latter effect remains as a determining factor for C_g in the high-pressure, high-velocity regions. To verify this hypothesis, we conducted plate-height measurements at a pressure of 57 kg/cm² (CO_2 carrier) and velocities up to 15 cm/sec. Columns packed with Sil-O-Cel of varying size were examined.

The results are plotted in Figs. 9 and 10. It can be seen that the slopes for *n*-pentane differ widely for packings of different size, whereas they did not in the experiments at atmospheric pressure.

Assuming that at high pressures and velocities the C term is additively built up from a stationary phase contribution independent of d_p (as discussed before) and an intraparticle gas-phase con-

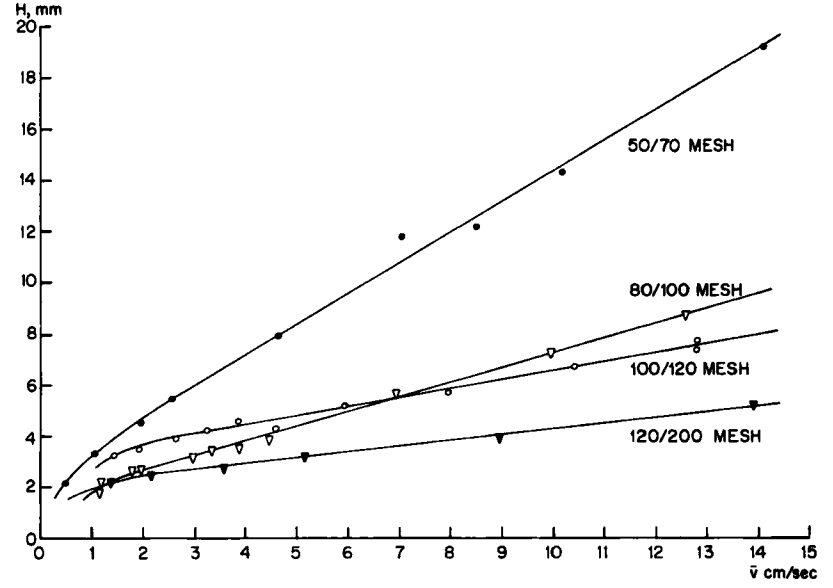

FIG. 9. Plate-height curves at a carbon dioxide pressure of 57 kg/cm² for *n*-pentane as a solute (columns B–E; T, 40°C).

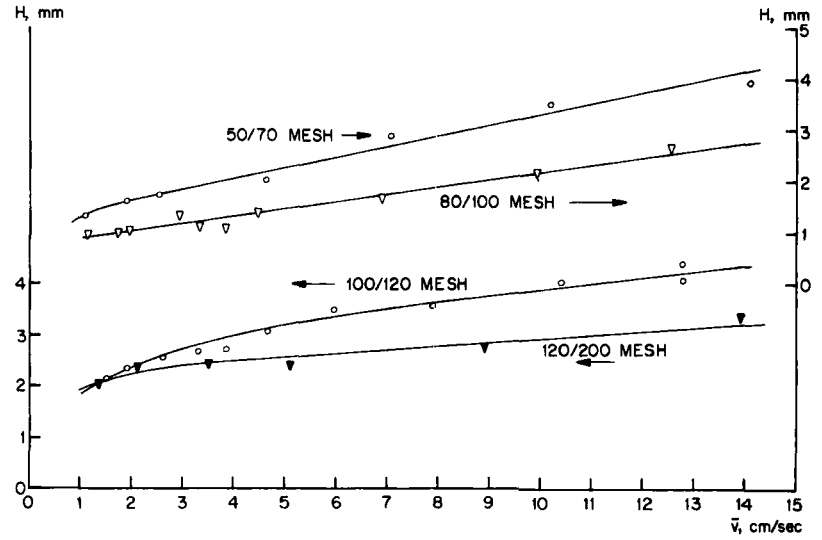

FIG. 10. Plate-height curves at a carbon dioxide pressure of 57 kg/cm² for methane as a solute (columns B–E; T, 40°C).

tribution proportional to d_p^2 [see Eq. (6)], it follows that C will be a linear function of d_p^2 if particle size only is varied. This is confirmed by the experimental results shown in Fig. 11.

To verify the above hypothesis further, we have entered the

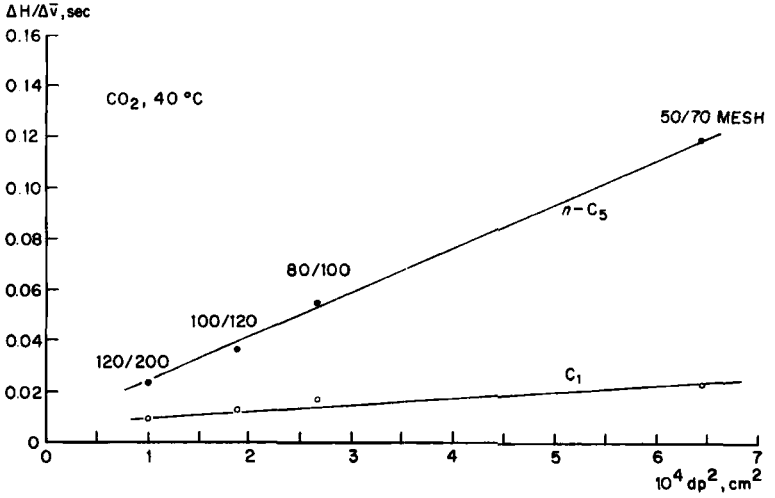

FIG. 11. Effect of particle size on the slope of the plate-height curves at a pressure of 57 kg/cm². Velocity range, 4–14 cm/sec (columns B–E).

TABLE 4

Relationship between the Coefficient of the Gas Contribution to the Nonequilibrium Term and Particle Diameter. Comparison between Theory and Experiment[a]

Solute	k'	D_g, cm²/sec	C_g, sec	
			Theory	Experimental
n-Pentane	4.5	8.4×10^{-4}	170 d_p^2	172 d_p^2
Methane	≈0	1.9×10^{-3}	23 d_p^2	26 d_p^2

[a] Carrier gas, CO_2; P, 57 kg/cm²; T, 40°C; velocity range, 4–14 cm/sec (d_p in cm).

intraparticle gas-phase contributions calculated from Eq. (6) with $\phi \simeq 0.5$, $\epsilon_p \simeq 0.5$ (mean values for columns B to E; see Table 1) and $q = 1.3$ (value used before) in Table 4 and compared them with the experimental C_g data obtained from Fig. 11. As can be seen, the agreement is very satisfactory.

Figure 11 also enables an estimate to be made of the liquid mass-transfer contributions at a pressure of 57 kg/cm² by extrapolation to $d_p^2 = 0$. The value found, $C_l \simeq 8 \times 10^{-3}$ sec for *n*-pentane, is about one-half the corresponding value at atmospheric pressure. Although the limited accuracy does not permit us to draw definite conclusions, it seems possible that C_l is lowered by the solution of CO_2 in squalane. Under the prevailing conditions, approximately 15 wt. % of CO_2 dissolves in squalane [cf. our earlier work (*1*)]. As discussed before, this may have resulted in a reduced viscosity and a correspondingly increased diffusivity.

For methane, C_l should theoretically be zero. However, the experimental line for C_l in Fig. 11 does not pass through the origin, as is theoretically required. A possible cause may be the finite response time of the detecting systems, considering that very narrow peaks are here involved (cf. experimental section).

Separating Efficiency of Packed Columns Operated with Supercritical Mobile Fluids

As we deduced from our earlier work on the pressure dependence of partition coefficients, chromatography with supercritical mobile fluids may offer attractive possibilities for the separation of heavy substances. The experimental work here discussed primarily served to study the role of various parameters, notably of carrier gas pressure, on plate height. Although the experiments at

this stage have not yet covered the field of specific interest, i.e., chromatography with a mobile fluid at both temperatures and pressures beyond the critical values, they enable a few deductions to be made concerning the separating potential of this form of chromatography.

From the previous discussions it will be clear that in the region of interest the main factors determining column efficiency are associated with packing nonuniformity, intraparticle gaseous diffusion, and liquid diffusion. We shall discuss the first two contributions only, since the role of the last one is not different from that in conventional GLC.

Effect of Packing Inhomogeneity. The effect of nonuniformity of the packing, which is less important at high velocities,* can in principle be reduced by improvement of the technique of column preparation. Alternatively, it can be minimized by reducing the column diameter. As follows from Eq. (9), a decrease in column diameter together with a reduction by the same factor in particle size (which is beneficial for the C term, as will be discussed later) lowers the profile contribution correspondingly. The columns A and B of 6 mm i.d. packed in a conventional way with particles of about 250 μ have been shown to possess an "A term" of the order of 2 mm. Hence, a column of 1 mm i.d. with particles of about 40 μ (325/400 mesh) should have an A term of only 0.3 mm if the degree of packing inhomogeneity can be kept the same. The preparation of such a column should be quite feasible, although the possibility of using it in chromatography with supercritical fluids depends upon the availability of suitable injection and detection systems.

The above extrapolation of the present work is beautifully confirmed by the recent experimental results of Myers and Giddings (35) which were published after conclusion of our experiments. Although their work is not strictly comparable to ours since the high pressure is not maintained over the full length of the column (the outlet being at atmospheric pressure), their results are of immediate interest since they used columns of about 0.5 mm i.d. filled with particles around 13 μ. With helium as a carrier gas at inlet pressures up to about 170 atm, minimum plate heights between about 0.1 and 0.4 mm were measured for methane and butane. Very recently, the same authors have extended their work to the very

* Whereas the intraparticle gaseous diffusion term increases in proportion to velocity, the contribution of packing inhomogeneity does not.

respectable inlet pressures of 2000 atm (*36*). It is shown that with increasing inlet pressure (and correspondingly higher flow rates) the plate height for such a column does not increase beyond about 0.4 mm.

Effect of Finite Rate of Diffusion. The effect of intraparticle diffusion is especially important at high fluid velocities. It is, therefore, the main obstacle to rapid and efficient separations. From Fig. 11 it can be inferred that with particles somewhat smaller than 100 μ, C is about 10^{-2} sec, which is of the same order as that found for the columns operated under normal GLC conditions. The use of such (or even finer) packing should be quite feasible. High-pressure gases and superficial fluids have low viscosities (compared with liquids), and, moreover, there is no serious objection to a fairly large pressure drop since few additional experimental difficulties are involved.

We therefore anticipate chromatography with supercritical fluids to be comparable to conventional gas chromatography as regards separation efficiency and speed.

In the same respects, chromatography with supercritical fluids will be superior to liquid chromatography. The latter technique is limited by pressure drop to a far greater extent due to the considerably smaller liquid diffusivities and the higher liquid viscosities.

Nomenclature

A, B, C	constants in simplified van Deemter equation
C_g	coefficient of first-order term in plate-height equation $[H = f(\bar{v})]$ pertaining to effects located in gas phase
C_l	coefficient of first-order term in plate-height equation, pertaining to effects located in the liquid phase
D_g	diffusion coefficient in gas phase
D_l	diffusion coefficient in liquid phase
d	sphere diameter
d_l	effective liquid film thickness
d_p	average particle diameter
d_s	equivalent sphere diameter (= diameter of a sphere with the same ratio of area to volume as the packing considered)
g	gravity constant
H	height equivalent to a theoretical plate
h	additive contribution to H

K	coefficient of permeability
k'	capacity ratio (= ratio of amounts of solute in stationary and mobile phases)
P	pressure
$\bar{P}$	average pressure
P_i	inlet pressure
P_o	outlet pressure
q	tortuosity factor (diffusion in micropores)
R	tube radius
Re	Reynolds number = $d_p\bar{v}\rho/\eta$
S_v	specific surface per unit volume of particle
u	nominal velocity (velocity calculated on empty tube)
$\bar{u}$	average nominal velocity
$\bar{v}$	average interstitial velocity
x	coordinate in axial direction
γ, γ_R	tortuosity factor (diffusion in interstitial channels)
ΔP	pressure drop across column
ϵ	porosity (volume of interstitial voids per unit volume of bed)
ϵ_p	particle porosity (volume of intraparticle pores per unit volume of particle)
η	dynamic viscosity
κ	dimensionless constant depending on geometry and relating to a velocity profile
λ_R	dimensionless constant pertaining to convective lateral mixing
ρ	density
ϕ	ratio of intragranular gas volume to total gas volume
φ	function
ψ	resistance coefficient

Acknowledgment

The authors wish to thank Mr. W. van Beersum, who carried out most of the measurements.

REFERENCES

1. S. T. Sie, W. van Beersum, and G. W. A. Rijnders, *Separation Sci.*, **1**, 459 (1966).
2. J. H. Knox, *J. Chem. Soc.*, **1961**, 433.
3. J. C. Giddings, *Anal. Chem.*, **37**, 60 (1965).
4. B. H. Sage and W. N. Lacey, *Some Properties of the Lighter Hydrocarbons,*

Hydrogen Sulfide and Carbon Dioxide, API Research Project 37, American Petroleum Institute, New York, 1956.
5. E. L. Quinn and C. L. Jones, *Carbon Dioxide*, American Chemical Society Monograph, Reinhold, New York, 1936.
6. *Bulletin FF-101*, Johns-Manville Corporation, New York, 1962.
7. W. J. Baker, E. H. Lee, and R. F. Wall, in *Gas Chromatography* (H. J. Noebels, R. F. Wall, and N. Brenner, eds.), Academic Press, New York, 1961.
8. E. R. Gilliland, *Ind. Eng. Chem.*, **26**, 681 (1934).
9. O. Hirschfelder, C. F. Curtiss, and R. B. Bird, *Molecular Theory of Gases and Liquids*, Wiley, New York, 1954, pp. 634–646.
10. J. H. Arnold, *J. Am. Chem. Soc.*, **30**, 3937 (1930).
11. Landolt-Börnstein, *Physikalisch-chemische Tabellen*, Springer, Berlin, 1923.
12. P. C. Carman, *Flow of Gases through Porous Media*, Butterworth, London, 1956.
13. A. E. Scheidegger, *The Physics of Flow through Porous Media*, Macmillan, New York, 1957.
14. S. dal Nogare and Jen Chiu, *Anal. Chem.*, **34**, 890 (1962).
15. H. E. Rose, *Proc. Inst. Engrs. (London)*, **153**, 141 (1945).
16. H. E. Rose and A. M. A. Rizk, *Proc. Inst. Mech. Engrs. (London)*, **160**, 493 (1949).
17. N. C. Saha and J. C. Giddings, *Anal. Chem.*, **37**, 830 (1965).
18. N. C. Saha and J. C. Giddings, *Anal. Chem.*, **37**, 822 (1965).
19. D. M. Ottenstein, *J. Gas Chromatog.*, **1**, 11 (1963).
20. J. J. van Deemter, F. J. Zuiderweg, and A. Klinkenberg, *Chem. Eng. Sci.*, **5**, 271 (1956); D. H. Desty, A. Goldup, and B. H. F. Whyman, *J. Inst. Petrol.*, **45**, 295 (1959).
21. S. Ergun, *Chem. Eng. Progr.*, **48**, 227 (1952).
22. M. J. E. Golay, in *Gas Chromatography* (D. H. Desty, ed.), Butterworth, London, 1958, p. 36.
23. R. Kieselbach, *Anal. Chem.*, **33**, 23 (1961).
24. J. Bohemen and J. H. Purnell, *J. Chem. Soc.*, **1961**, 2630.
25. D. D. Deford, R. J. Lloyd, and B. O. Ayers, *Anal. Chem.*, **35**, 426 (1963).
26. J. C. Giddings and P. D. Schettler, *Anal. Chem.*, **36**, 1483 (1964).
27. R. H. Perrett and J. H. Purnell, *Anal. Chem.*, **35**, 430 (1963).
28. J. C. Giddings, *Anal. Chem.*, **33**, 962 (1961).
29. R. B. Evans, G. M. Watson, and E. A. Mason, *J. Chem. Phys.*, **35**, 2076 (1961).
30. S. T. Sie and G. W. A. Rijnders, *Anal. Chim. Acta*, **38**, 3 (1967).
31. F. H. Huyten, W. van Beersum, and G. W. A. Rijnders, in *Gas Chromatography* (R. P. W. Scott, ed.), Butterworth, London, 1960, p. 224.
32. A. B. Littlewood, paper presented at the *5th International Symposium on Gas Chromatography, Brighton, 1964.*
33. J. C. Giddings, *Nature*, **184**, 357 (1959).
J. C. Giddings, *Anal. Chem.*, **34**, 1186 (1962).
34. D. S. Horne, J. H. Knox, and L. McLaren, *Separation Sci.*, **1**, 531 (1966).
35. M. N. Myers and J. C. Giddings, *Anal. Chem.*, **38**, 294 (1966).
36. M. N. Myers and J. C. Giddings, *Separation Sci.*, **1**, 761 (1966).

Received by editor August 28, 1967
Submitted for publication October 18, 1967